Photorefractive beam-fanning effect and self-pulsations in coated $LiNbO_3$ slabs

Georgy Zartov, Tihomir Tenev, Krassimir Panajotov, Evgeny Popov, and Rumiana Peyeva

Institute of Solid State Physics, Bulgarian Academy of Sciences, 72 Tzarigradsko Chaussee Boulevard, 1784 Sofia, Bulgaria

Hugo Thienpont and Irina Veretennicoff

Department of Applied Physics and Photonics, Vrije Universiteit Brussel, Pleinlaan 2, B-1050 Brussels, Belgium

Received August, 14 2000; revised manuscript received November 6, 2000; accepted November 6, 2000.

We investigate the dynamical behavior of optical Fabry–Perot resonators consisting of $LiNbO_3$ slabs (x and c cut) that are coated with different (absorbing or lossless) dielectric multilayers deposited on both sides of the slabs. Bistable switching is observed experimentally. The buildup of beam fanning with time leads to destructive interference for a portion of the incident beam, inducing a change in absorption and heating, hence to switching off. As a result, self-pulsations appear whose frequency depends strongly on the input light intensity, the spot size, and the focusing. Switching and self-pulsations are not observed in the case of lossless coatings or for bare $LiNbO_3$ slabs, although strong photorefractive beam fanning is still present. We also study the influence of the incident-beam characteristics (width and focusing) on the beam-fanning process and the pulsating behavior. © 2001 Optical Society of America

OCIS codes: 310.1620, 190.1450, 190.4870, 190.5330, 190.4420, 230.5440.

1. INTRODUCTION

$LiNbO_3$ is a classical photorefractive material.[1,2] When a focused incident laser beam (an Ar^+ or a He–Ne laser) falls upon an uncoated $LiNbO_3$ slab, we observe a typical beam-fanning effect, i.e., a single incident beam of light generates a fanned-out profile of scattering. The beam fanning originates from energy coupling between the incident beam and the scattered beam. Scattering occurs because of surface roughness, refractive-index inhomogeneity, impurities in solids, and so forth.[3] The scattered beam will overlap with the incident one even if it has a finite transverse cross section. Because the scattered beam has a large number of spatial components, this overlap leads to the formation of a large number of photoinduced gratings. Depending on the crystal orientation, some of the spatial components may be amplified by the incident beam as a result of the power transfer in two-beam coupling. Even with quite low initial scattering the amplified light can be quite significant. For a laser beam of moderate power the scattered light increases over time and eventually reaches a steady-state scattering pattern.[3] The question of whether beam fanning is caused by amplified noise[4] or by amplified spatial frequencies of the beam itself[5] is still open.

Brown and Valley[6] numerically demonstrated a beam-fanning effect by modeling the propagation of two Gaussian beams through a two-dimensional photorefractive medium with and without internal scattering (noise). They obtained the angular distribution of the field for different penetration depths into the photorefractive medium by taking the Fourier transform with respect to the transverse coordinate. A pronounced widening of the angular spectrum was found for noisy media.

A numerical study[7] was also performed in which many pairs of two-wave-mixing interactions were taken into account to model the time development of the fanning effect. The angular profile of the fanning dynamics revealed that the amplitudes of the higher-angular components grew slower over time until a stationary pattern was formed.

In more recent papers[8,9] the rigorous coupled-wave diffraction theory was used to simulate the exact dynamical behavior of two-wave and multiwave mixing in photorefractive materials. The influence of the refractive-index mismatch, the ratio of the incident signal-to-pump amplitudes, and the length of the crystal on light diffraction was demonstrated. This time-dependent approach demonstrated that the dynamical behavior (oscillatory or nonoscillatory and even possibly chaotic) depended critically on the sample length.

In this paper, we investigate beam-fanning effects in a photorefractive medium ($LiNbO_3$) inside a nonlinear Fabry–Perot resonator. Nonlinear resonators have been studied extensively in the field of digital optical processing.[10–15] Different interference-filter constructions that act as bandpass filters,[10,11] bistable etalons with absorbed transmission,[12] and double-half-wave filters[15] have been examined. In each of these structures part of the incident light is absorbed, which generates a temperature rise inside the filter and modulates the optical constants of the thermo-optic nonlinear layers. In this way, internal feedback is realized, and the well-known phenomenon of thermal optical bistability is observed.[16–20]

One way to control the polarization state of the emerging light is to include anisotropy within the optical cavity. Polarization-sensitive resonators open up new perspectives on polarization optical bistability and polarization

switching and routing.[21–24] Such devices can be implemented as logic gates in polarization-based optical processors in which the information is encoded and controlled by use of the vectorial character of light.[22–25] The behavior of different polarization-bistable anisotropic interference filters (with and without heat sinks) has been investigated experimentally,[26] confirming the existence of polarization-driven all-optical bistability. The stationary results show good agreement with the numerical predictions obtained by a coupled thermo-optic multilayer model.[27]

The introduction of both photorefractive and absorbing materials inside the cavity essentially modifies the dynamical response of the resonator because, even at relatively low incident powers (10–100 mW), the thermo-optic effect and the photorefractive effect take place simultaneously. The aim of this paper is to present new experimental results on the dynamical behavior of interference structures with a photorefractive central layer and to point out possible ways of describing this behavior.

2. EXPERIMENTAL RESULTS

We investigate structures of the type

$$(\mathrm{HL})^N(m\mathrm{M})(\mathrm{LiNbO_3})(m\mathrm{M})(\mathrm{LH})^N,$$

where the layers H (ZnS) and L (Na_3AlF_6) are nonabsorptive quarter-wave (either at Ar^+ or He–Ne laser wavelengths) layers with high and low refractive indices, respectively, N is an integer that represents the number of (HL) periods in the stack ($N = 2$ or $N = 3$), and (mM) represents the absorptive (ZnSe, $m = 8$) or the nonabsorptive (ZnS, $m = 1$) m-multiple quarter-wave layer. The $LiNbO_3$ slabs are c or x cut with a thickness of 0.7–1.0 mm. The surrounding medium is air ($n = 1$). Filters with different numbers of periods N are manufactured to compare the influence of mirror reflectivity. The two (mM) layers can be either absorptive or lossless to clarify the influence of self-heating. Samples with a glass plate (~1.0 mm thick) instead of a $LiNbO_3$ slab that have a similar finesse are also manufactured to clarify the role of photorefractivity.

The presence of absorptive layers on both sides of the central layer leads to a temperature change that is proportional to the absorbed optical power. The consequent changes in the optical thicknesses in the multilayer are determined by the temperature distribution and depend on the amount of power absorbed during the characteristic time for thermoconduction. This characteristic time depends on different parameters (the specific thermocapacity, the medium density, the coefficient of thermoconductivity, and the radius of the incident laser beam). Experimentally, all-optical bistable switching is observed in our structures. The hysteresis width depends on the polarization orientation of the incident linearly polarized light as well as on the orientation of the anisotropic medium. It also depends on the angle of incidence.[28] Self-pulsations of the transmitted intensity I_{out} are observed experimentally for a constant input intensity I_{in} from an Ar^+ laser (λ=514.5 nm).

Figure 1 shows the transmitted light intensity plotted as a function of the input intensity. The appearance of self-pulsations in the switched-on state is clearly visible. In Fig. 2 different types of self-pulsations are shown for a constant input intensity.

Such types of self-pulsation with a frequency of 1–2 Hz for similar experimental conditions and input intensities have been observed many times. Their shape depends strongly on the input intensity, the focusing f, the angle of incidence θ, and the reflectivity of the resonator ($N = 2$ or $N = 3$). Because of this high sensitivity to the experimental conditions, it is difficult to reproduce a particular type of self-pulsation.

In Fig. 3 a set of frames shows a typical space distribution of transmitted light during self-pulsations. Two cycles of self-pulsations are captured with a CCD camera over the course of 2 s. In frames 8 and 23 the moment of the switching ON (the high-transmission state) is clearly visible. Afterward the transmitted light spot stretches along the c axis of the $LiNbO_3$ crystal, which causes a gradual decrease in the transmission and passage into

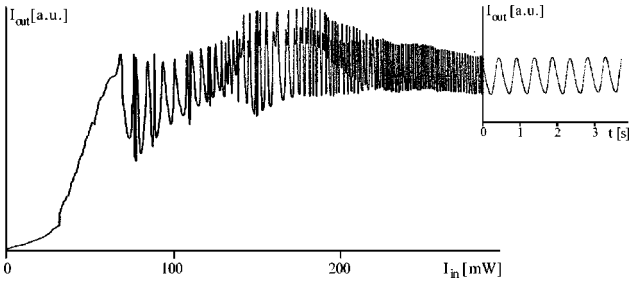

Fig. 1. Output intensity I_{out} plotted versus the input intensity I_{in}. Self-pulsations appear in the switched-on state. The inset shows self-induced pulsations in time at a constant input intensity I_{in}. The structure was $(HL)^3(8M)(LiNbO_3)(8M)(LH)^3$. The $LiNbO_3$ was x cut; $\lambda = 514.5$ nm; M denotes ZnSe; $f = 70$ mm.

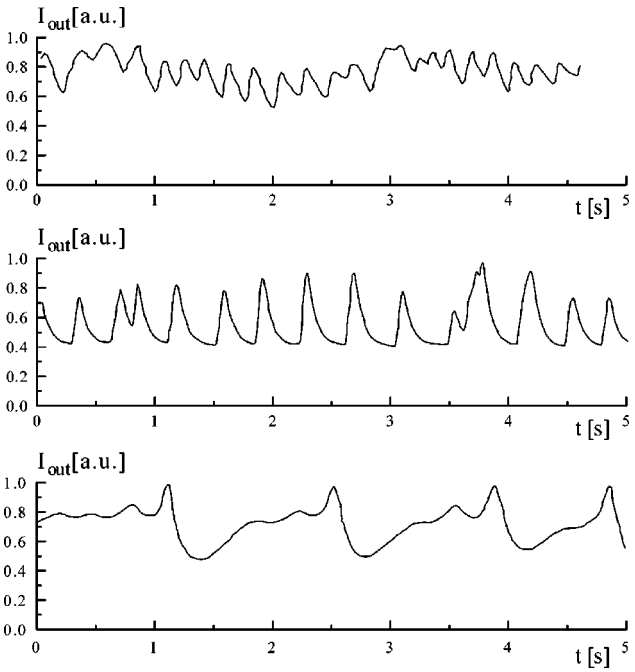

Fig. 2. Particular realizations of pulsations of the output intensity I_{out} over time. The structure was $(HL)^3(8M)(LiNbO_3)(8M)(LH)^3$. The $LiNbO_3$ was x cut; $\lambda = 514.5$ nm; M denotes ZnSe; $f = 70$ mm.

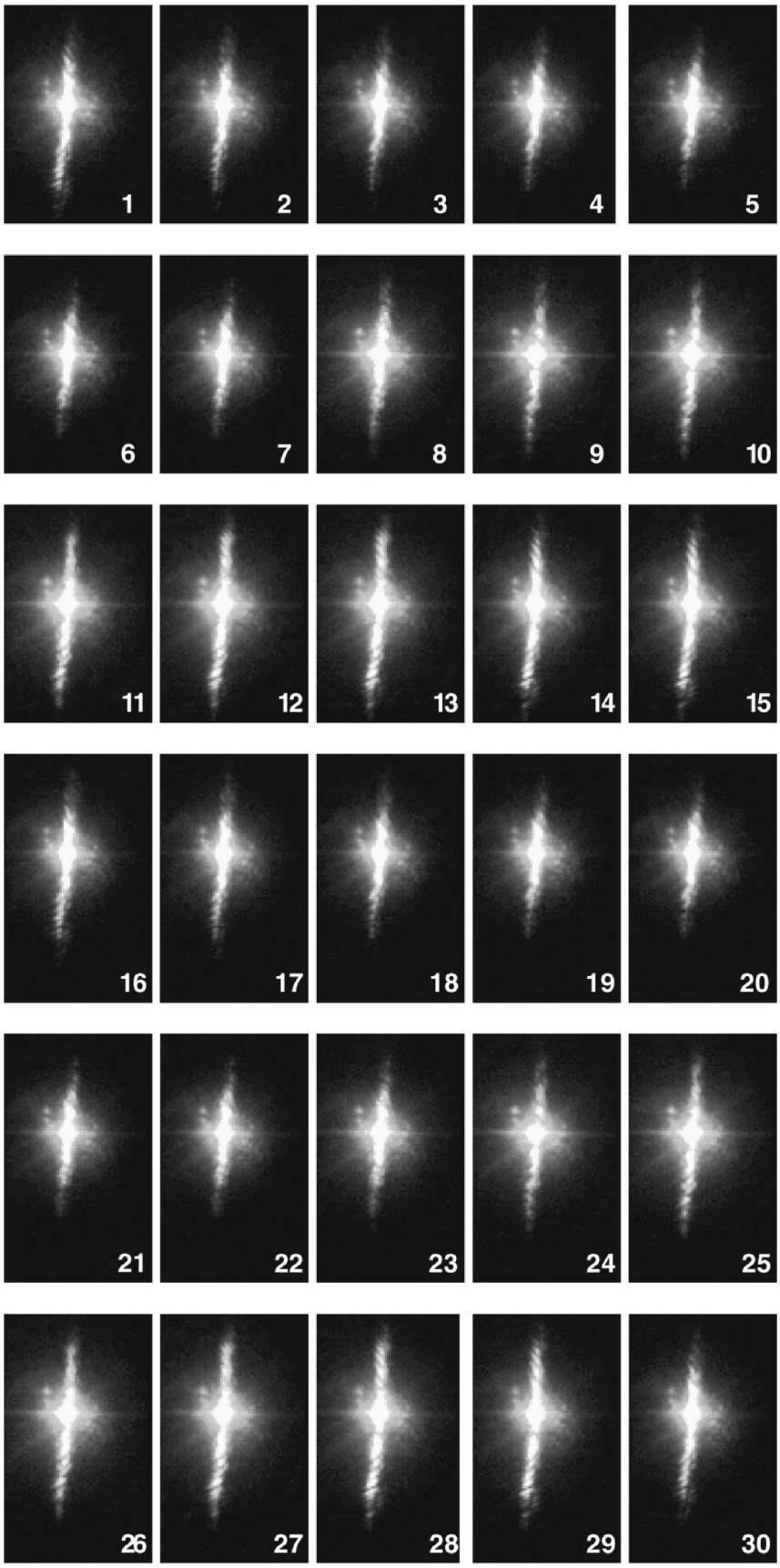

Fig. 3. Space distribution of the light transmitted through the sample in a self-pulsating regime. Thirty frames were captured with a CCD camera over the course of 2 s. The structure was $(HL)^3(8M)(LiNbO_3)(8M)(LH)^3$. The $LiNbO_3$ was x cut; $\lambda = 514.5$ nm; M denotes ZnSe; $f = 70$ mm; $I_{in} = 100$ mW; $\theta = 1.3°$.

the switched-off state (the low-transmission state). The sample is irradiated with extraordinary-polarized light of $I_{in} \sim 100$ mW from an Ar^+ laser with λ=514.5 nm.

The spatiotemporal behavior of the transmitted light shows that self-pulsations are observed in only filters with $LiNbO_3$ *x*-cut slabs. To further prove this observation, we examine bare $LiNbO_3$ samples.

An uncoated $LiNbO_3$ slab with a thickness of 0.7 mm is illuminated with extraordinary-polarized light from a He–Ne laser ($I_{in} = 2$ mW). Figure 4 shows a photograph of the beam-fanning profile on a screen that is 40 mm behind the sample for normal incidence. The beam is focused through a lens with a focal length of $f = 70$ mm.

The frames shown in Fig. 5 illustrate the time development of the beam-fanning profile on a screen that is positioned 80 mm behind the sample at normal incidence. The beam is focused through a lens of $f = 250$ mm. It can be seen that the time development of the profile is completed in approximately 20 s under these conditions.

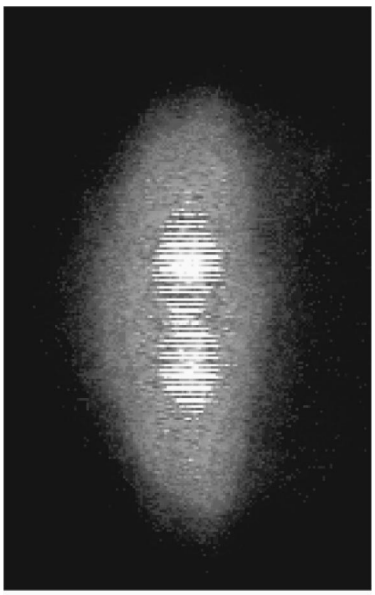

Fig. 4. Space distribution, after the development of the beam-fanning process, of the transmitted light behind a 0.7-mm $LiNbO_3$ *x*-cut slab that was irradiated by extraordinary light from a He–Ne laser ($\lambda = 632.8$ nm; $I_{in} = 20$ mW; $f = 70$ mm) at normal incidence.

The beam profile is continuously being stretched along the crystal's *c* axis in a manner that is symmetrical relative to the initial spot of the beam. In the case of tight focusing (Fig. 4), the stretching is more pronounced, and the beam splits into two spots.

The same kind of symmetrical beam-fanning patterns, whose size depends on the beam waist and the power, were shown by Liu *et al.*[29] They analyzed steady-state (Gaussian) beam fanning in $LiNbO_3$ (from the nonlinearly coupled Kukhtarev equations) by including both diffusive and photovoltaic effects and by heuristically adding thermal effects into the calculation. The overall induced refractive-index change, $\Delta n(x, y, z)$, for extraordinary-polarized light is expressed[29] (if one dominant electrostatic field along the *c* axis from the photovoltaic effect is assumed) by

$$\Delta n = (\Delta n)_{DIFF} + (\Delta n)_{PV} + (\Delta n)_{TH} = 1/2 n_e^3 r_{33}(E_{DIFF_1} + E_{PV_1}) + (dn/dT)\Delta T,$$

where n_c is the extraordinary refractive index, r_{33} is the relevant electro-optic coefficient, (dn/dT) is the thermo-optic coefficient, and the subscripts DIFF, PV, and TH denote diffusive, photovoltaic, and thermal, respectively. By solving four coupled equations, Liu *et al.*[29] showed that the diffraction and the thermal effects modify the beam in both transverse dimensions, whereas the diffusive and the photovoltaic effects occur along only the optic axis. Their experimental and numerical results show an approximately symmetric far-field intensity profile because the dominant refractive-index changes that result from the photovoltaic and the thermal effects are symmetric. In addition, both the photovoltaic effects and the thermal effects increase with the light intensity.

Our subsequent experiments were performed with coated (absorbing and lossless) $LiNbO_3$ *c*- and *x*-cut slabs. Absorbing (8-multiple quarter-wave) layers were formed to create enough heat to obtain low-power bistable switching. The reason for using the various samples is to understand the origin of the observed self-pulsations—thermal, photorefractive, or a combination of the two.

Bistable switching (and self-pulsations) were not obtained for uncoated samples or for samples with nonabsorbing layers, even for the case of $LiNbO_3$ *x*-cut slabs in which significant beam-fanning effects were present.

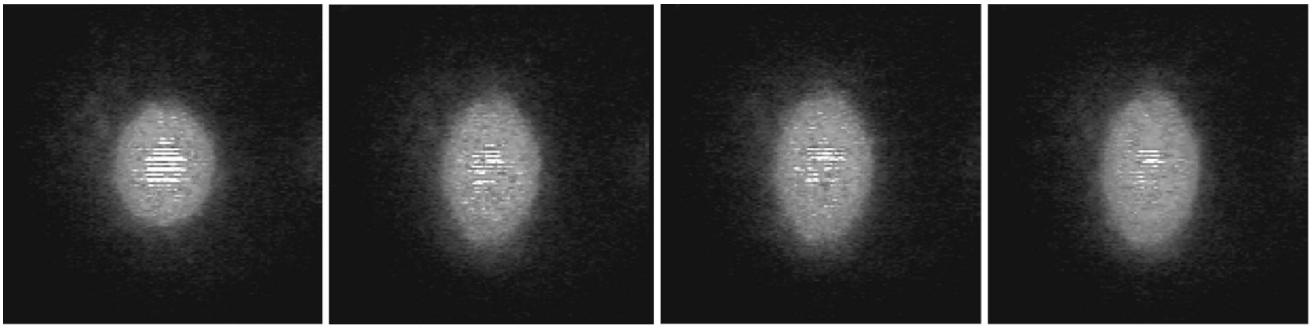

Fig. 5. Space distribution of the transmitted light behind a 0.7-mm $LiNbO_3$ *x*-cut slab that was irradiated by extraordinary light from a He–Ne laser ($\lambda = 632.8$ nm; $I_{in} = 20$ mW; $f = 250$ mm) at normal incidence for (a) 0 s, (b) 20 s, (c) 40 s, (d) 60 s after the beginning of irradiation.

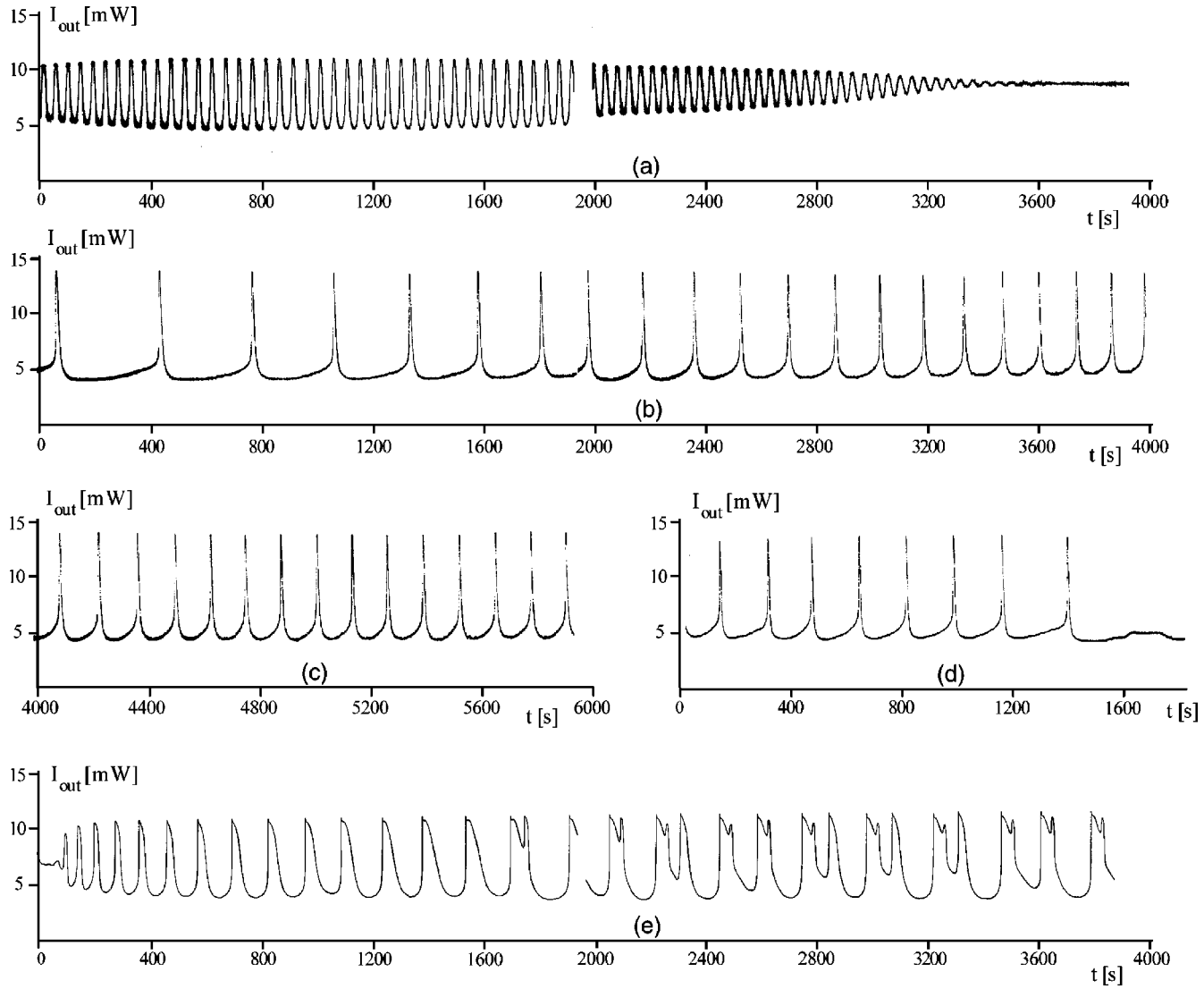

Fig. 6. Self-pulsations of the transmitted intensity at a constant input intensity. The samples had a central layer of x-cut $LiNbO_3$ and absorptive coatings and were irradiated by a focused He–Ne laser light of $\lambda = 632.8$ nm and $I_{in} = 20$ mW: (a) Ordinary-polarized light with $f = 250$ mm and $\theta = 1.35°$. (b) Extraordinary-polarized light with $f = 250$ mm and $\theta = 0.76°$. (c) This plot is a continuation of plot (b). (d) Extraordinary-polarized light with $f = 250$ mm and $\theta = 0.73°$. (e) Extraordinary-polarized light with $f = 500$ mm and $\theta = 2.3°$. The structure of the sample was $(HL)^3(8M)(LiNbO_3)(8M)(LH)^3$. The $LiNbO_3$ was x cut, and M denotes ZnSe.

These experiments show that the level of internal feedback is not sufficient to cause all-optical switching, i.e., beam fanning, by itself, does not cause optical bistability in the considered structures.

In the case of absorbing layers on a slab of glass or c-cut $LiNbO_3$, only bistable switching was observed by our continually changing either the incident-light intensity or the incident angle. However, self-pulsations were not observed in these samples. In these experiments, we varied the incident laser beam focusing in a wide range from $f = 1000$ mm to as low as $f = 15$ mm. We must note here that there is no noticeable beam fanning in the case of a $LiNbO_3$ c-cut slab.

Self-pulsations are observed for only x-cut samples of $LiNbO_3$ (for which substantial beam fanning exists) and for absorbing layers (for which all-optical switching exists). Figure 6 represents experimentally recorded (on an X–Y recorder) self-pulsations of the transmitted intensity at a constant input intensity. A focused He–Ne laser beam is incident at different angles. It is surprising to see that, in Fig. 6(a), we still register self-pulsations because, for this crystal-axis orientation and incident-light polarization, the beam fanning of the $LiNbO_3$ is more than tenfold weaker.[29] The form of the self-pulsations depends critically on the incident angle, e.g., changing it by only $\sim 0.03°$ results in an increase in the period and the disappearance of the self-pulsations [Fig. 6(d)].

The strong dependence of the dynamical behavior on the angle of incidence is a result of the high mirror reflectivity and the thick $LiNbO_3$ slab that yield a small half-width filter resonance. In our experiments the incident angle is in the vicinity of the first transmission resonance. This angle varies as a result of the wedge of the $LiNbO_3$ slab. Consequently, the resonance is located at different angles with respect to normal incidence. The orientation of the wedge relative to the crystal axis and the plane of

incidence also influences the conditions for interference in comparison with a perfectly parallel slab.

We simulated the dynamical behavior of our structures by taking into account light absorption and heating but not beam fanning in the case of an anisotropic photorefractive layer in the structure. We used an algorithm that is analogous to the coupled thermo-optical multilayer model.[27] The temperature and the power distributions were found by the simultaneous solution of the heat equation and Maxwell's equations. The optical part computes the power distribution, the absorption, and the changes in the refractive indices and the layer thicknesses during heating, assuming an instantaneous response of the power distribution to the change in the temperature distribution. The slab (glass or $LiNbO_3$) was divided into a number of sublayers (200 or 300), and a linear thermo-optical effect and thermal expansion were assumed. The thermal part calculates both the longitudinal and the transverse temperature distributions inside the thick slab. The time evolution of the temperature profile along the beam was calculated by use of the model of Abraham and Halley.[30]

Two absorbing mirrors were considered to be two thin thermal layers with thermal sources inside (with Gaussian radial distributions). These simulations did not show any instabilities or self-pulsations of the transmitted intensity, although we varied the thermal constants of the layers across a broad range. We attribute this result to the large thermal-diffusion time of all the layers (including the slab) so that the temperature response of the multilayer structure was much slower than the optical response (the cavity build-up time). The lack of pulsations in the simulations is in agreement with our experiments—we did not observe such self-pulsations in samples with a glass or a $LiNbO_3$ *c*-cut slab for which no beam fanning was present.

We find that the modal theory of Haelterman and Vitrant[31,32] is most appropriate for the description and the modeling of the observed bistability and self-pulsations. This theory greatly simplifies the numerical study of transverse effects and provides a deep understanding of the physical phenomena that are related to optical bistability, especially the roles of diffraction and the angle of incidence on the behavior of nonlinear Fabry–Perot etalons. On the basis of this theory and by use of linear stability analysis dynamical regimes that correspond to self-pulsing, frequency doubling, and chaos have been investigated.[33–37]

Our experiments on $LiNbO_3$ *x*-cut crystals without coatings are illustrated in Figs. 4 and 5 (also see Refs. 6, 7, and 29) and show that beam fanning broadens the angular spectrum of the transmitted laser beam. The corresponding defocusing and its time of development are proportional to the beam intensity. The beam-fanning behavior is similar in $LiNbO_3$ *x*-cut samples that have either absorbing or lossless coatings. This similarity can be seen from the frames of Fig. 3. The amount of fanning (defocusing) and the corresponding time for its development are proportional to the intracavity intensity. Hence coupling of the modal theory to the heat equation will make possible the correct modeling of the observed dynamical behavior.

3. CONCLUSION

Experimental results have been presented that demonstrate the appearance of self-plusations of transmitted light for the case of a $LiNbO_3$ *x*-cut resonator with absorbing layers in the mirrors. Such self-pulsations are absent in cases of similar $LiNbO_3$ *c*-cut and glass resonators, although bistable switching is still present. This finding shows that all-optical bistable switching has to be combined with photorefractive beam fanning to explain the observed dynamical behavior.

ACKNOWLEDGEMENTS

This paper benefited from the project "Investigation of the role of the polarization of light in photonic devices for optical information processing" that was conducted by the Belgium Foundation for Science (FWO) and the Bulgarian Academy of Sciences.

Address correspondence to G. Zartov at the address on the title page or e-mail, zart@issp.bas.bg.

REFERENCES

1. A. Ashkin, G. D. Body J. M. Dziedzig, R. G. Smith, A. A. Ballman, J. J. Levenstein, and K. Nassan, "Optically induced refractive index inhomogeneities in $LiNbO_3$ and $LiTaO_3$," Appl. Phys. Lett. **9**, 72–74 (1966).
2. T. J. Hall, R. Jaura, L. M. Connor, and P. D. Foote, "The photorefractive effect—a review," Prog. Quantum Electron. **10**, 77–146 (1985).
3. P. Yeh, *Introduction to Photorefractive Nonlinear Optics* (Wiley, New York, 1993).
4. V. V. Voronov, I. R. Dorosh, Yu. S. Kuz'minov, and N. V. Tkachenko, "Photoinduced light scattering in BSN:Ce crystals," (in Russian) Kvant. Elektron. (Moscow) **7**(11), 2313–2318 (1980).
5. J. Feinberg, "Asymmetric self-defocusing in an optical beam from the photorefractive effect," J. Opt. Soc. Am. **72**, 46–51 (1982).
6. W. P. Brown and G. C. Valley, "Kinky beam paths inside photorefractive crystals," J. Opt. Soc. Am. B **10**, 1901–1906 (1993).
7. M. Snowbell, M. Horowitz, and B. Fischer, "Dynamics of multiple two-wave mixing and fanning in photorefractive materials," J. Opt. Soc. Am. B **11**, 1972–1982 (1994).
8. J. Jarem and P. P. Banerjee, "Exact, dynamical analysis of the Kukhtarev equations in photorefractive barium titanate using rigorous coupled-wave diffraction theory," J. Opt. Soc. Am. A **13**, 819–831 (1996).
9. J. Jarem and P. P. Banerjee, "A nonlinear, transient analysis of two- and multi-wave mixing in a photorefractive material using rigorous coupled-wave diffraction theory," Opt. Commun. **123**, 825–842 (1996).
10. F. V. Karpushko and G. V. Sinitzyn, "An optical logic element for integrated optics in a nonlinear semiconductor interferometer," (in Russian) Zh. Prikl. Spektrosk. **29**, 1323–1326 (1978).
11. S. D. Smith, J. G. H. Mathew, M. R. Taghizadeh, A.C. Walker, B. S. Wherrett, and A. Hendry, "Room temperature, visible wavelength optical bistability in interference filters," Opt. Commun. **51**, 357–362 (1984).
12. A. C. Walker, "Reflection bistable etalons with absorbed transmission," Opt. Commun. **59**, 145–150 (1986).
13. S. D. Smith, A. C. Walker, B. S. Wherrett, F. A. P. Tooley, J. G. H. Mathew, M. R. Taghizadeh, and I. Janossy, "Cascadable digital optical logic circuit elements in the visible and infrared: demonstration of some first all-optical circuits," Appl. Opt. **25**, 1586–1593 (1986).

14. B. S. Wherrett, D. Hutchings, and D. Russell, "Optically bistable interference filters: optimization consideration," J. Opt. Soc. Am. B **3**, 351–362 (1986).
15. A.C. Hutchings, C. H. Wang, and B. S. Wherrett, "Optically bistable interference filters: self-consistent modeling of nonlinear optical characteristics and optimization," J. Opt. Soc. Am. B **8**, 618–631 (1991).
16. R. W. Eason and A. Miller, eds., *Nonlinear Optics in Signal Processing*, Engineering Aspects in Lasers Series, T. A. Hall, ed. (Chapman & Hall, London, 1993).
17. P. Mandel, S. D. Smith, and B. S. Wherrett, eds., *Optical Bistability Towards Optical Computing: The European Joint Optical Bistability Project* (North-Holland, Amsterdam, 1987).
18. I. Janossy, M. R. Taghizadeh, J. G. H. Mathew, and S. D. Smith, "Thermally induced optical bistability in thin-film devices," IEEE J. Quantum Electron. **QE-21**, 1447–1452 (1985).
19. I. Janossy, J. G. H. Mathew, E. Abraham, and S. D. Smith, "Dynamics of thermally induced optical bistability," IEEE J. Quantum Electron. **QE-22**, 2224–2229 (1986).
20. H. Thienpont, W. Peiffer, I. Veretennicoff, C. De Tandt, W. Ranson, R. Vounckx, and A. Koster, "Optical logic planes with SIlicon IMpanted OXide technology: a first step towards low-cost smart pixels," in *Proceedings of the International Conference on Frontiers in Information Optics,* T. Asakura, ed., Kyoto, Japan, 4–8 April 1994, p. 293.
21. I. P. Areshev, T. A. Murina, N. N. Rosanov, and V. K. Subashiev, "Polarization and amplitude optical multistability in a nonlinear ring cavity," Opt. Commun. **47**, 414–419 (1983).
22. A. Korpel and A. W. Lohmann, "Polarization and optical bistability," Appl. Opt. **25**, 1528–1529 (1986).
23. A. W. Lohmann, "Polarization and optical logic," Appl. Opt. **25**, 1594–1597 (1986).
24. N. I. Zheludev, "Polarization instabilities and multistabilities in nonlinear optics," (in Russian) Usp. Fiz. Nauk **154**(4), 683–717 (1989).
25. M. Pelt, H. Thienpont, and I. Veretennicoff, "Aspects of cascadability and logic of polarization bistable Fabry–Perot resonators," in *Technical Digest of the Fifth European Quantum Electronics Conference EQEC'94* (Institute of Electrical and Electronics Engineers, New York, 1994), p. 65.
26. K. Panajotov, T. Tenev, G. Zartov, M. Pelt, J. Danckaert, H. Thienpont, and I. Veretennicoff, "Polarization driven polarization bistability in anisotropic interference filters," J. Nonlinear Opt. Phys. Mater. **5**, 351–365 (1996).
27. K. Panajotov, T. Tenev, R. Peyeva, M. Pelt, J. Danckaert, H. Thienpont, and I. Veretennicoff, "Coupled thermo-optic multilayer model for intensity and polarization switching in interference filters," Bulg. J. Phys. **24**, 143–155 (1997).
28. G. Zartov, T. Tenev, K. Panajotov, R. Peyeva, J. Danckaert, H. Thienpont, and I. Veretennicoff, "Angular dependencies of thermo-optic bistable switching in interference filters," in *Proceedings of the Tenth ISCMP Conference "Thin Film Materials and Devices—Developments in Science and Technology,* " J. M. Marshall, N. Kirov, A. Vavrek, and J. M. Maud, eds. (World Scientific, Singapore, 1998), pp. 473–476.
29. J.-J. Liu, P. P. Banerjee, and Q. Wang Song, "Role of diffusive, photovoltaic, and thermal effects in beam fanning in $LiNbO_3$" J. Opt. Soc. Am. B **11**, 1688–1693 (1994).
30. A. Abraham and J. M. Halley, "Some calculations of temperature profiles in thin films with laser heating," Appl. Phys. A: Solids Surf. **42**, 279–285 (1987).
31. M. Haelterman, G. Vitrant, and R. Reinisch, "Transverse effects in nonlinear planar resonators. I. Modal theory," J. Opt. Soc. Am. B **7**, 1309–1318 (1990).
32. G. Vitrant, M. Haelterman, and R. Reinisch, "Transverse effects in nonlinear planar resonators. II. Modal analysis for normal and oblique incidence," J. Opt. Soc. Am. B **7**, 1319–1327 (1990).
33. M. Haelterman and G. Vitrant, "Drift instability and spatiotemporal dissipative structures in a nonlinear Fabry–Perot resonator under oblique incidence," J. Opt. Soc. Am. B **9**, 1563–1570 (1992).
34. M. Neviere, E. Popov, R. Reinisch, and G. Vitrant, *Electromagnetic Resonances in Nonlinear Optics* (Gordon & Breach, London, 2000).
35. J. Danckaert and G. Vitrant, "Modulational instabilities in diffusive Kerr-type resonators," Opt. Commun. **104**, 196–206 (1993).
36. J. Danckaert, G. Vitrant, R. Reinisch, and M. Georgiou, "Nonlinear dynamics in single-mode optical resonators," Phys. Rev. A **48**, 2324–2333 (1993).
37. J. Danckaert, "Nonlinear planar resonator for optical processing: simple models, including stratification, time, and polarization," Ph.D. dissertation (Vrije Universiteit, Brussels, Belgium, 1992).